ORIGINAL ARTICLE

Mitral chordae tendineae force profile characterization using a posterior ventricular anchoring neochordal repair model for mitral regurgitation in a three-dimensional-printed *ex vivo* left heart simulator

Michael J. Paulsen [a], Annabel M. Imbrie-Moore[a,b], Hanjay Wang[a], Jung Hwa Bae [b],
Camille E. Hironaka[a], Justin M. Farry [a], Haley J. Lucian[a], Akshara D. Thakore[a], John W. MacArthur Jr[a],
Mark R. Cutkosky [b] and Y. Joseph Woo[a,c,*]

[a] Department of Cardiothoracic Surgery, Stanford University, Stanford, CA, USA
[b] Department of Mechanical Engineering, Stanford University, Stanford, CA, USA
[c] Department of Bioengineering, Stanford University, Stanford, CA, USA

* Corresponding author. Departments of Cardiothoracic Surgery and Bioengineering, Stanford University, Falk Cardiovascular Research Building CV-235, 300 Pasteur Drive, Stanford, CA 94305-5407, USA. Tel: +1-650-7253828; fax: +1-650-7360901; e-mail: joswoo@stanford.edu (Y.J. Woo).

Received 15 May 2019; received in revised form 19 August 2019; accepted 26 August 2019
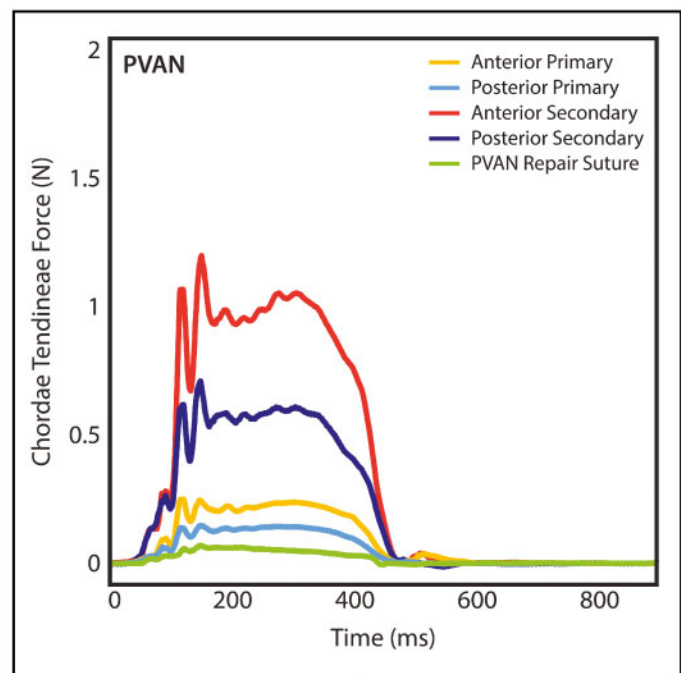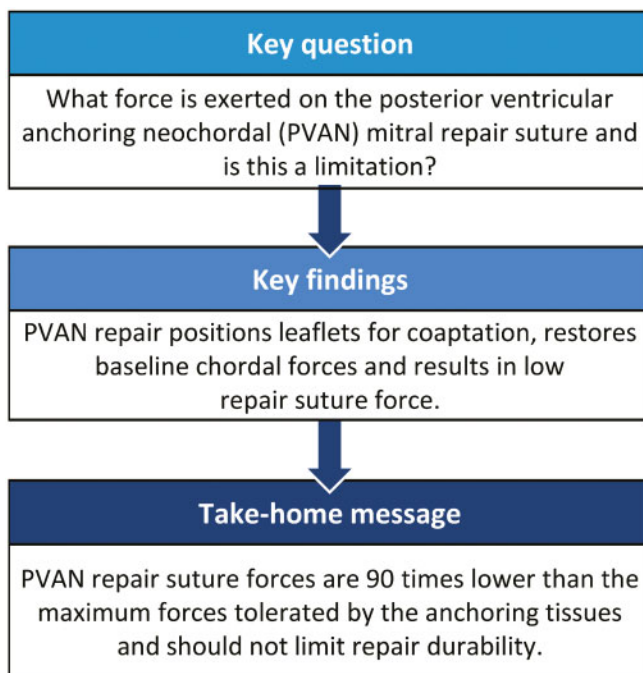
Abstract

OBJECTIVES: Posterior ventricular anchoring neochordal (PVAN) repair is a non-resectional technique for correcting mitral regurgitation (MR) due to posterior leaflet prolapse, utilizing a single suture anchored in the myocardium behind the leaflet. This technique has demonstrated clinical efficacy, although a theoretical limitation is stability of the anchoring suture. We hypothesize that the PVAN suture positions the leaflet for coaptation, after which forces are distributed evenly with low repair suture forces.

METHODS: Porcine mitral valves were mounted in a 3-dimensional-printed heart simulator and chordal forces, haemodynamics and echocardiography were collected at baseline, after inducing MR by severing chordae, and after PVAN repair. Repair suture forces were measured with a force-sensing post positioned to mimic *in vivo* suture placement. Forces required to pull the myocardial suture free were also determined.

RESULTS: Relative primary and secondary chordae forces on both leaflets were elevated during prolapse ($P < 0.05$). PVAN repair eliminated MR in all valves and normalized chordae forces to baseline levels on anterior primary (0.37 ± 0.23 to 0.22 ± 0.09 N, $P < 0.05$), posterior primary (0.62 ± 0.37 to 0.14 ± 0.05 N, $P = 0.001$), anterior secondary (1.48 ± 0.52 to 0.85 ± 0.43 N, $P < 0.001$) and posterior secondary chordae (1.42 ± 0.69 to 0.59 ± 0.17 N, $P = 0.005$). Repair suture forces were minimal, even compared to normal primary chordae forces (0.08 ± 0.04 vs 0.19 ± 0.08 N, $P = 0.002$), and were 90 times smaller than maximum forces tolerated by the myocardium (0.08 ± 0.04 vs 6.9 ± 1.3 N, $P < 0.001$).

DISCUSSION: PVAN repair eliminates MR by positioning the posterior leaflet for coaptation, distributing forces throughout the valve. Given extremely low measured forces, the strength of the repair suture and the myocardium is not a limitation.

Keywords: Mitral valve repair • Chordae tendineae forces • Biomechanics • Mitral valve surgery

---

ABBREVIATIONS

FBG	Fibre Bragg Grating
LV	Left ventricular
MR	Mitral regurgitation
PTFE	Polytetrafluoroethylene
PVAN	Posterior ventricular anchoring neochordal
SAM	Systolic anterior motion

INTRODUCTION

Since being reported in the 1950s, mitral valve repair has become a highly reproducible and effective treatment for degenerative mitral regurgitation (MR) in even the most complex valvular lesions [1–6]. Many techniques exist ranging from extensive resections to elaborate geometric reconstructions to completely non-resectional techniques [7–9]. Resection is highly effective, but minor drawbacks include being irreversible and time-consuming for complex repairs. In addition, overly aggressive resection may result in monoleaflet function, whereas insufficient resection may result in systolic anterior motion (SAM) [10–12]. Neochordae replacement with polytetrafluoroethylene (PTFE) suture is oftentimes faster, but requires precise measurements to ensure a proper coaptation plane and prevention of SAM [13, 14]. More extensive and complex techniques can also be more challenging in minimally invasive approaches. To remedy some of these drawbacks, we have previously described a simplified, non-resectional leaflet-remodelling technique whereby redundant, prolapsing leaflet tissue is imbricated to create a smooth coaptation surface to repair degenerative MR [15–17]. Because this repair keeps potentially diseased chordal tissue in place, it carries the theoretical risk of continued chordal elongation resulting in SAM or late prolapse. A further iteration on this technique that was first described in the 'European Journal of Cardio-Thoracic Surgery' in 2013—the posterior ventricular anchoring neochordal (PVAN) repair—remedied this risk by using a single suture to anchor the remodelled posterior leaflet to the posterior left ventricular (LV) wall (Fig. 1A) [18]. This technique has proven to be highly effective and particularly useful in minimally invasive approaches, though some concern has been raised about the stability of the suture anchored in the posterior myocardium as opposed to the typical neochord anchoring location in the fibrous portion of a papillary muscle. We hypothesize,

however, that the PVAN repair suture serves primarily to position the leaflet posteriorly for proper coaptation and to prevent SAM (Fig. 1B), after which point systolic forces will be evenly distributed throughout the mitral valve apparatus due to the structural optimization provided by imbrication of excess leaflet tissue, resulting in low peak forces on the PVAN repair suture and the underlying myocardial anchoring point (Fig. 1C and D). In this study, we used a novel 3-dimensional (3D)-printed *ex vivo* left heart simulator with high-fidelity fibre-optic force sensors with embedded Bragg gratings to validate our theory.

MATERIALS AND METHODS

Left heart simulator

We designed a customized left heart chamber and prototyped the device using 3D printing (Carbon M2, Carbon3D Inc., Redwood City, CA, USA) and milling, which we have previously described (Fig. 2A) [19, 20]. Briefly, the chamber was mounted to a pulsatile linear actuator (ViVitro Superpump, ViVitro Labs, Victoria, BC, Canada) and outfitted with left atrial, ventricular and aortic pressure transducers (Utah Medical Products Inc., Midvale, UT, USA), as well as electromagnetic flow probes (Carolina Medical Electronics Inc., East Bend, NC, USA) in the mitral and aortic positions. Normal saline was used as our test fluid to ensure proper flow probe transduction. Compliance chambers in the aortic root and aortic positions, as well as a viscoelastic impedance adapter, allowed precise tuning of the waveforms. In the aortic position, a 29-mm mechanical aortic valve (St. Jude Regent, Abbott Vascular, Lake Bluff, IL, USA) was placed. Using a 28-mm leakless disc valve (ViVitro) in the mitral position as our reference valve, the system was tuned to generate physiological pressure and flow waveforms with systolic pressure of 120 mmHg, diastolic pressure of 80 mmHg and cardiac output of 5 l/min.

Sample preparation

Fresh porcine hearts were obtained from a local abattoir and the mitral valve apparatus was dissected free, including the papillary muscles and chordae tendineae. Only valves with intercommissural distances of 34–36 mm were included ($n = 8$). A 5-mm cuff of left atrium was left in place and used to sew the valves to 3D-printed elastomeric sewing rings that modelled the shape and material properties of the native mitral annulus.
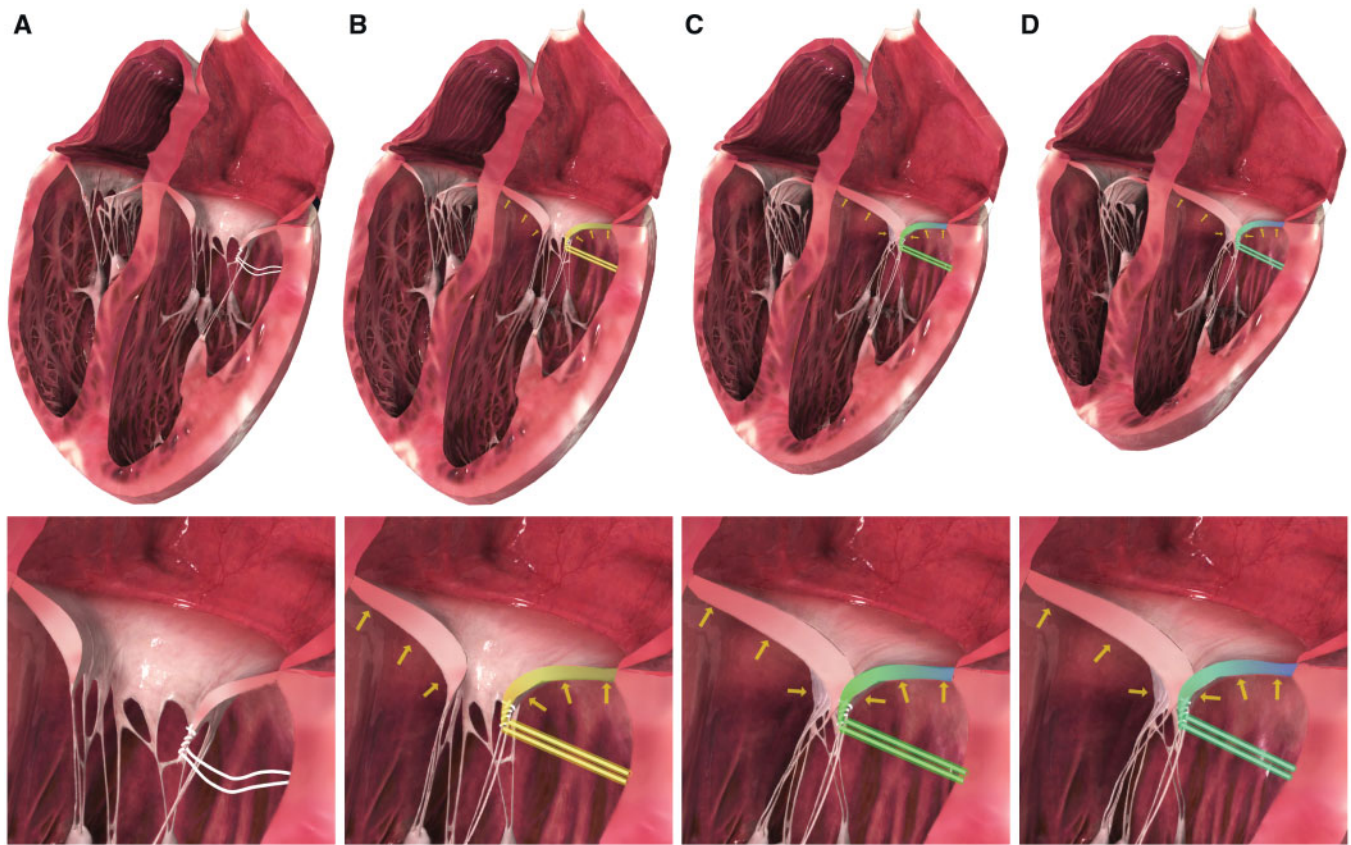
Figure 1: Rendered illustration of the posterior ventricular anchoring neochordal (PVAN) repair and the hypothesized forces experienced on the repair suture throughout the cardiac cycle. During diastole (**A**), the PVAN suture is relaxed and experiences no tension. As systole begins (**B**), the closing posterior leaflet is held in position for optimal coaptation by the PVAN repair suture. Forces on the PVAN suture peak immediately before leaflet coaptation. Once the anterior and posterior leaflets coapt (**C**), the forces on the PVAN suture begin to fall as the leaflet forces are distributed throughout the 2 opposing leaflets (**D**). Images modified with permission and licensed from 3D4Medical Ltd.
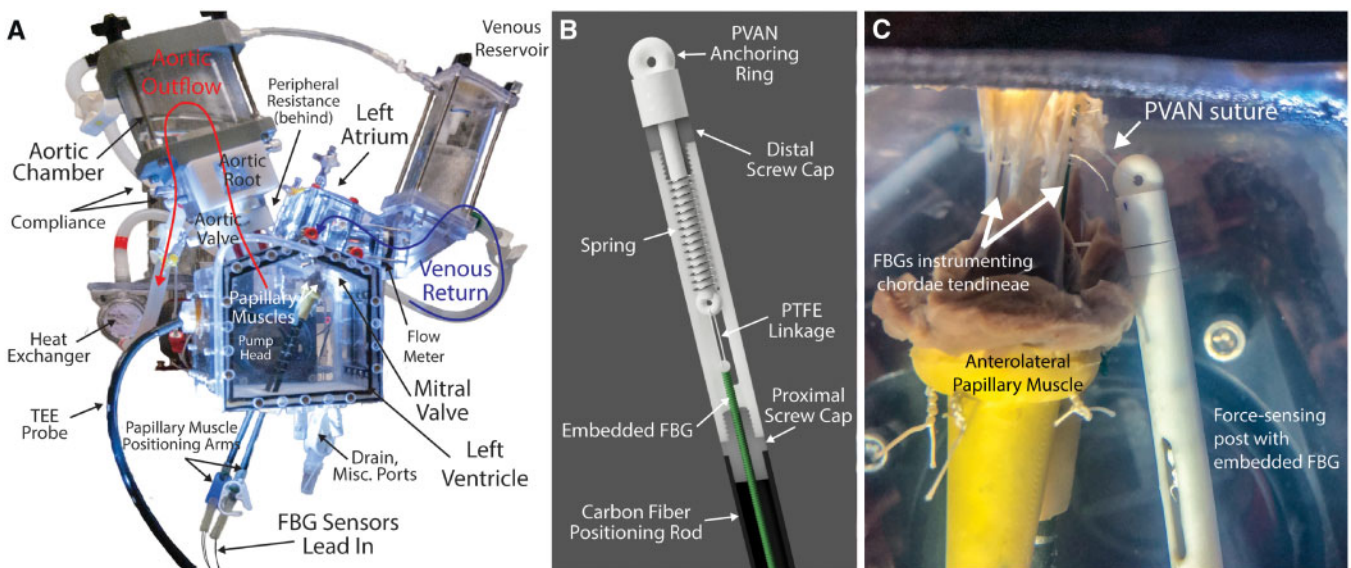
Figure 2: (**A**) Schematic of the Stanford Left Heart Simulator with each major component labelled. Reprinted with permission from [21]. Copyright 2019 Elsevier. (**B**) Computer-aided design rendering of the force-sensing post with embedded FBG sensor for measuring strain on the PVAN repair suture. (**C**) *Ex vivo* experimental set-up showing the PVAN repair suture anchored to the force-sensing post with embedded FBG sensor, which has been positioned to mimic the correct *in vivo* placement of the PVAN repair suture. FBG: Fibre Bragg Grating; PTFE: polytetrafluoroethylene; PVAN: posterior ventricular anchoring neochordal; TOE: transoesophageal echocardiography.

Importantly, the native mitral annulus was not directly attached to the sewing ring, so as not to overly limit the motion of the native annulus, hence the reason for using the cuff of the left atrium to attach the valves to the sewing rings. The valves were first tacked to the sewing ring in the proper position with 6–8 interrupted horizontal mattress sutures using 2-0 braided polyester suture, followed by a continuous running 2-0 polypropylene suture line sealing the left atrial cuff and sewing ring. The papillary muscles were sewn to silicone sewing pads with pledgeted 2-0 braided polyester suture; the papillary muscle pads were inserted onto the ends of carbon fibre positioning rods, which passed into the chamber through spherical compression gaskets allowing for adjustment.

Posterior ventricular anchoring neochordal and chordae tendineae force measurements

We developed customized chordae tendineae force sensors with high accuracy and a small footprint using Fibre Bragg Grating (FBG) sensors, which we have described previously [20]. Briefly, FBGs are optical fibres with a series of spatial period gratings that reflect a particular wavelength of light transmitted by an optical interrogator. When tensile or compressive strain is applied, the space between the gratings changes, altering the reflected wavelength. The wavelength shift is directly proportional to strain, which can be calibrated to force applied. Using FBGs as a base structure, we developed an outer shell that allows for reusable attachment of the sensors to chordae. For each valve tested, multiple chordae were instrumented with FBGs (5–6 per valve), including a range of anterior, posterior, primary and secondary chordae. PTFE suture (CV-5 or CV-7, depending on chordae size) was used to sew the sensors to the chordae proximally and distally to the sensor. Once attached, the chordae segment between the sutures was cut, allowing the sensor to transmit the entire chordae load. As the mitral apparatus was dissected from the native hearts and mounted in the simulator, no LV wall was present to use for PVAN anchoring. Instead, we created a 3D-printed force-sensing post to simultaneously measure forces on and position the PVAN suture (Fig. 2B). The anchoring post was positioned between the papillary muscles ∼10 mm posterior and 10 mm inferior to the P2 segment of the posterior leaflet.

Supplementary experiments explored how measured forces on the suture correspond to the ultimate strength of the suture anchoring point in the LV wall. Porcine myocardium (n = 6) was explanted from the posterior LV wall, between the papillary muscles inferior to the annulus. A CV-5 PTFE suture was passed into the myocardium to an approximate depth of 3–4 mm and then loosely tied in accordance with the PVAN technique. The myocardium was then secured between 2 textured plates to prevent unnatural bowing of the tissue. The plates included an opening through which the suture could be accessed and tensioned. The suture pull-out tests were performed using an Instron 5848 Microtester (Norwood, MA, USA) with a 100 N load cell. Preconditioning occurred at 0.4 mm/s to an amplitude of 2 mm; the suture was then pulled at 0.4 mm/s until LV wall failure occurred [21]. Tensile forces were continuously measured, and the maximum tensile force was recorded.

Study design and experimental set-up

We used an *ex vivo* model with a repeated-measures design, allowing each valve to serve as its own negative and positive

control. After the simulator was zeroed and tuned using the reference valve, experimental valves were mounted and force transducers were implanted. The system was filled with saline and allowed to reach 37°C before baseline haemodynamic, flow, force, echocardiographic and videometric data were collected. Without draining the circuit, P2 prolapse was induced by cutting several primary P2 chordae with minimally invasive instruments through an access port designed into the system. Two to four chordae were cut to obtain a regurgitant fraction between 20% and 40%. Data were then collected in the prolapse condition. Compliance and resistance were maintained for consistency. In the setting of acute MR, ventricular and aortic pressures decreased; for comparative purposes, prolapse forces were normalized to baseline maximum ventricular pressures during analysis. Next, valves were repaired using the PVAN technique with a CV-5 PTFE suture. The force-sensing post was positioned to mimic the location of the LV anchoring point (Fig. 2C), allowing for accurate placement of the PVAN suture whilst measuring forces. The PVAN suture was then passed through the posterior leaflet and used to imbricate the prolapsed segment before being tied. Given that the experimental valves had normal annular dimensions, ring annuloplasty was not performed to limit confounding factors influencing the repair. Data collection was repeated following repair.

Data acquisition and analysis

Haemodynamic data were acquired using a data acquisition system and included software (ViVitro). Strain measurements were measured with an optical interrogator (Micron Optics si255; Micron Optics, Atlanta, GA, USA) at 1000 Hz, and converted into forces using calibration plots obtained during sensor manufacture. Waveforms were imported into MATLAB (R2019a, MathWorks Inc., Natick, MA, USA) for signal processing, composite plotting and summary data generation. Summary data were imported into R for statistical analysis (R 3.6.0. with Jamovi 0.9.6.9). We used a linear mixed-model analysis fit by the restricted maximum-likelihood model with unadjusted post-hoc testing for multiple comparisons to statistically compare the groups using a repeated-measures design [22]. This technique allows for a repeated-measure design (in this case, taking measurements from the baseline condition, prolapse condition and repair condition) much like a repeated-measures ANOVA, but also allows the analysis to incorporate the clustering found from within each valve tested. Because each valve tested is different, which may influence the measurements taken from this valve, it is important to account for these differences. Lastly, because of anatomical considerations, it was not always possible to test an anterior primary, posterior primary, anterior secondary and posterior secondary chordae from each individual valve, resulting in missing values in the data. Repeated-measures ANOVA uses list-wise deletion to address missing data, which can result in significant bias, whereas linear mixed models do not. As such, bias can be reduced and power increased through the use of a linear mixed-model design. Experimental condition (grouped into baseline, prolapse and repair conditions) and chordae location (grouped into anterior primary, posterior primary, anterior secondary and posterior secondary) were the fixed effects and valve number was the random effect. Data are normal and homoscedastic unless
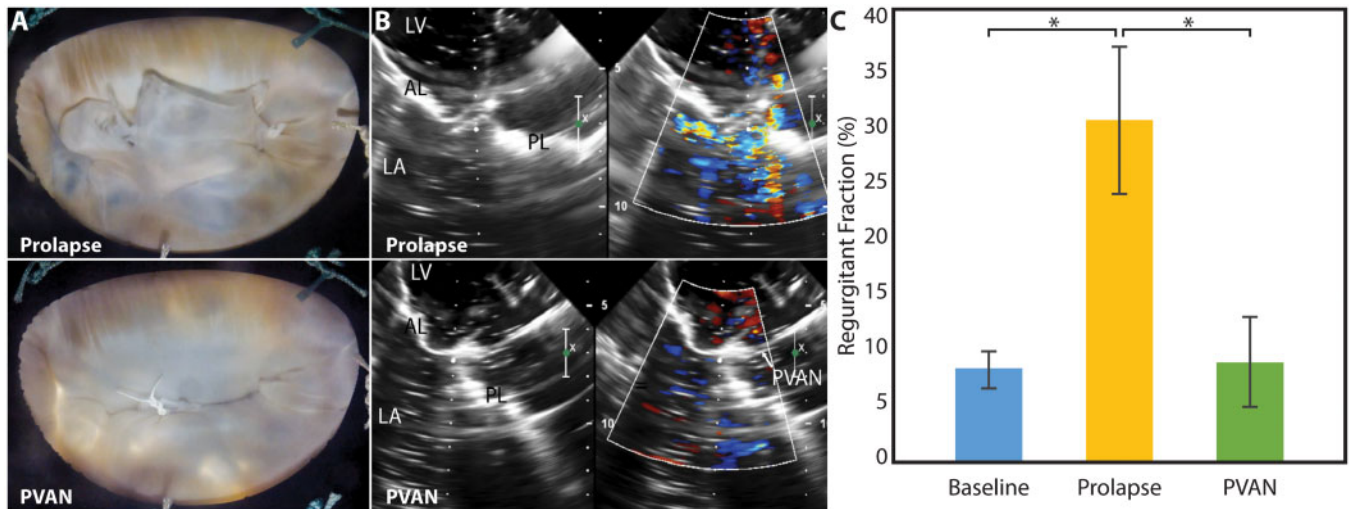
Figure 3: High-speed videography still frames of the mitral valve from the surgeons' view during prolapse (**A**, top) showing isolated P2 prolapse with ruptured (cut) chordae. Valve competency is restored following PVAN repair (**A**, bottom). Two-dimensional colour Doppler echocardiography images demonstrate moderate–severe mitral regurgitation (MR) secondary to posterior leaflet prolapse with an eccentric jet (**B**, top). PVAN repair corrected MR in all experiments. The repair suture attached to the force-sensing post can be appreciated in the echocardiography images after PVAN repair, with correction of posterior leaflet prolapse (**B**, bottom). Regurgitant fraction (**C**) measured by an electromagnetic flow probe demonstrates that PVAN repair effectively corrects MR to baseline levels ($8.4 \pm 1.5\%$ vs $30.3 \pm 6.5\%$ vs $9.1 \pm 4.0\%$). *$P < 0.001$. AL: anterior leaflet; LA: left atrium; LV: left ventricle; PL: posterior leaflet; PVAN: posterior ventricular anchoring neochordal.
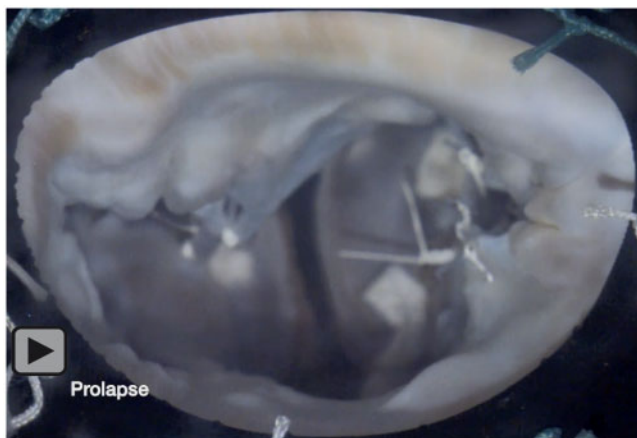
Video 1: High speed video demonstrating isolated P2 prolapse model of mitral regurgitation before and after posterior ventricular anchoring neochordal repair.

noted and are reported as mean ± standard deviation with a *P*-value <0.05 being considered significant.

RESULTS

The PVAN technique eliminated MR in all valves ($n = 8$). Visually, PVAN repair corrected P2 prolapse (Fig. 3A and Video 1), which was confirmed with echocardiography (Fig. 3B and Video 2). For more sensitive measurement of MR, regurgitant fraction was calculated from flow waveforms generated by the electromagnetic flow meters (Fig. 3C). Regurgitant fraction decreased from $30.3 \pm 6.5\%$ during prolapse to $9.1 \pm 4.0\%$ following PVAN repair ($P < 0.001$), which was equivalent to baseline levels in normal valves ($8.4 \pm 1.5\%$, $P = 0.79$). Gross haemodynamic parameters, including pressure and flow waveforms, are plotted in Fig. 4A and B. The shaded regions represent the standard deviation,
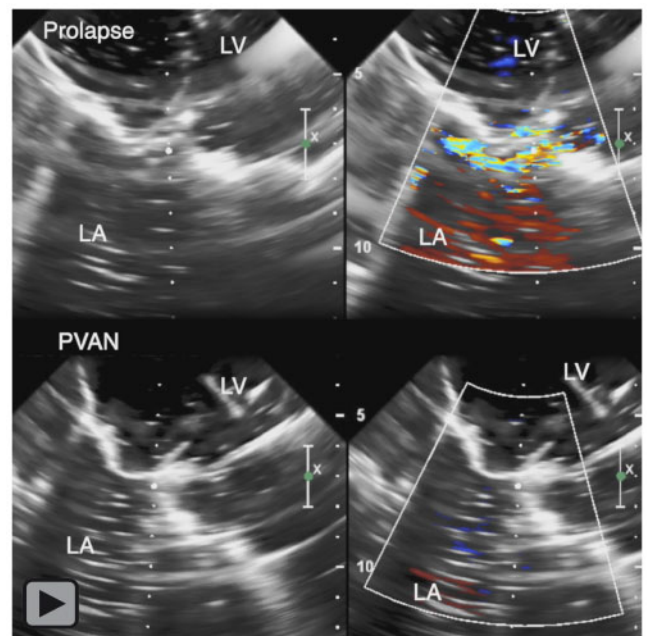
Video 2: Echocardiographic views of the mitral valve with color doppler prior to and after posterior ventricular anchoring neochordal repair.

which suggests that PVAN repair maintains baseline haemodynamic properties, as the tracings are superimposable. Other haemodynamic parameters are summarized in Table 1, demonstrating no significant difference in any parameters between baseline and following PVAN repair. PVAN did not have a restrictive effect on the mitral valve, as effective orifice area was maintained following PVAN repair versus baseline (6.8 ± 3.5 vs 4.5 ± 3.4, $P = 0.12$).

Composite force tracings are shown in Fig. 5. In the prolapse condition, as expected, forces normalized to ventricular pressure were significantly elevated versus baseline force measurements in
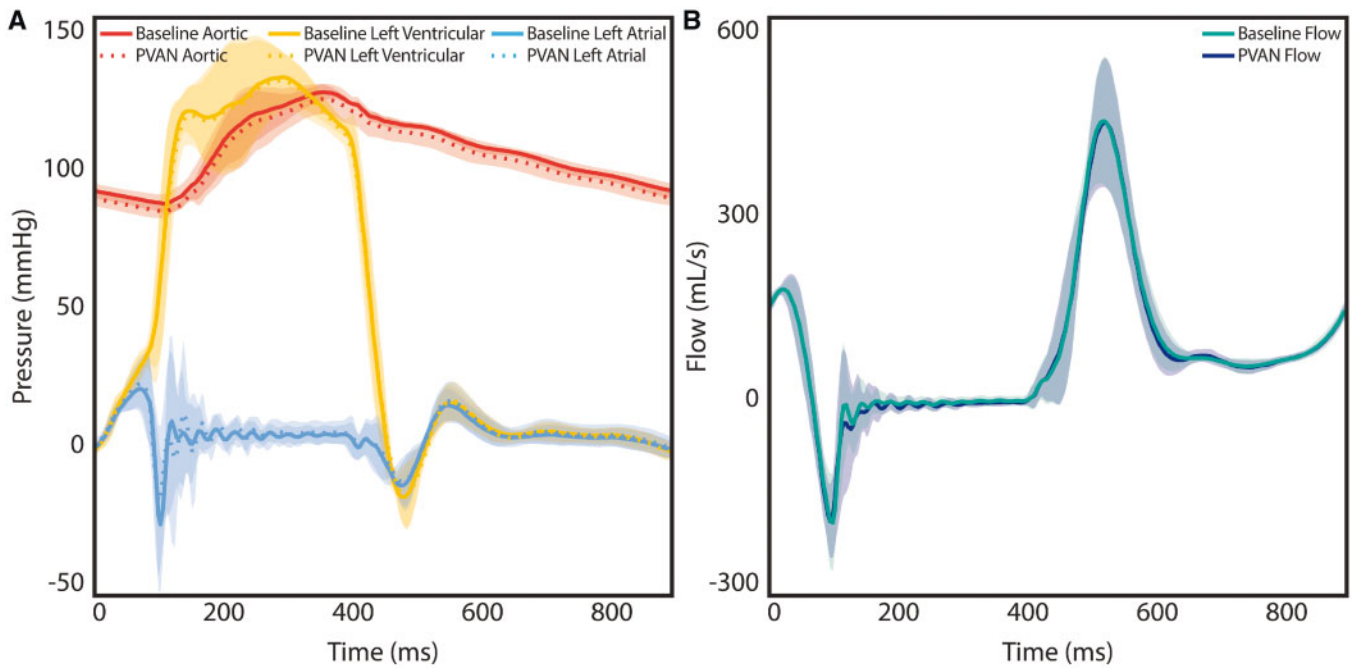
Figure 4: Composite pressure tracings (**A**) were indistinguishable between baseline and following PVAN repair, confirming restoration of aortic, left ventricular and left atrial pressures to baseline levels after PVAN repair. No significant difference was found in mean flow (**B**) between the baseline and PVAN repair groups. The shaded regions represent standard deviation. PVAN: posterior ventricular anchoring neochordal.

Table 1: Haemodynamic parameters and chordae tendineae force measurements

	Baseline (n = 8)	Prolapse (n = 8)	PVAN (n = 8)	P-value Baseline versus prolapse	Baseline versus PVAN repair	Prolapse versus PVAN repair
Haemodynamics						
Heart rate (bpm)	70.0 ± 0.0	70.0 ± 0.0	70.0 ± 0.0	1.000	1.000	1.0
Mean arterial pressure (mmHg)	100.2 ± 1.2	77.3 ± 9.7	97.6 ± 3.5	**<0.001**	0.395	**<0.001**
Systolic pressure (mmHg)	120.9 ± 2.1	95.4 ± 10.0	118.4 ± 4.9	**<0.001**	0.465	**<0.001**
Diastolic pressure (mmHg)	80.7 ± 2.1	60.9 ± 9.8	77.9 ± 2.3	**<0.001**	0.368	**<0.001**
Mean atrial pressure (mmHg)	5.9 ± 3.3	4.9 ± 2.6	6.5 ± 3.9	0.310	0.512	0.11
Mean ventricular pressure (mmHg)	50.7 ± 3.5	41.0 ± 4.6	50.1 ± 4.1	**<0.001**	0.696	**<0.001**
Maximum ventricular pressure (mmHg)	136.9 ± 14.3	112.2 ± 19.8	136.1 ± 13.9	**<0.001**	0.831	**<0.001**
Cardiac output (l/min)	4.5 ± 0.3	3.7 ± 0.7	4.5 ± 0.3	**<0.001**	0.923	**<0.001**
Effective stroke volume (ml)	64.9 ± 4.7	53.4 ± 9.8	64.7 ± 4.3	**<0.001**	0.923	**<0.001**
Pump stroke volume (ml)	103.5 ± 13.9	103.6 ± 13.9	103.5 ± 13.9	0.788	0.969	0.76
Mean transmitral pressure (mmHg)	0.3 ± 1.6	0.0 ± 1.7	1.3 ± 1.8	0.567	0.112	**0.039**
Mean transmitral back pressure (mmHg)	114.1 ± 10.5	88.7 ± 15.9	111.8 ± 9.9	**<0.001**	0.425	**<0.001**
Mitral forward flow time (s)	0.53 ± 0.02	0.51 ± 0.01	0.55 ± 0.03	**0.041**	0.194	**0.003**
Effective orifice area (cm^2)	6.8 ± 3.5	6.5 ± 3.3	4.5 ± 3.4	0.828	0.118	0.17
Mitral valve regurgitant fraction (%)	8.4 ± 1.5	30.3 ± 6.5	9.1 ± 4.0	**<0.001**	0.788	**<0.001**
Mitral forward volume (ml)	70.9 ± 5.2	76.3 ± 10.3	71.2 ± 4.6	**0.021**	0.877	**0.029**
Mitral closing volume (ml)	-5.5 ± 0.6	-7.1 ± 1.5	-6.0 ± 1.6	**0.029**	0.494	0.11
Mitral leakage volume (ml)	-0.5 ± 1.4	-15.7 ± 5.7	-0.5 ± 1.8	**<0.001**	0.984	**<0.001**
Mitral leakage rate (ml)	-1.8 ± 5.1	-55.5 ± 18.3	-2.0 ± 7.1	**<0.001**	0.974	**<0.001**
Transmitral leakage energy loss (mJ)	10.6 ± 22.5	182.1 ± 45.6	11.7 ± 30.0	**<0.001**	0.936	**<0.001**
Chordae tendineae forces						
Anterior primary (N)	0.23 ± 0.08	0.37 ± 0.23[a]	0.22 ± 0.09	**0.046**	0.791	**0.028**
Posterior primary (N)	0.14 ± 0.06	0.62 ± 0.37[a]	0.14 ± 0.05	**0.001**	0.978	**0.001**
Anterior secondary (N)	0.93 ± 0.38	1.48 ± 0.52[a]	0.85 ± 0.43	**<0.001**	0.520	**<0.001**
Posterior secondary (N)	0.76 ± 0.28	1.42 ± 0.69[a]	0.59 ± 0.17	**0.005**	0.376	**0.001**
PVAN repair suture (N)			0.08 ± 0.04			

[a]Prolapse chordae force measurements normalized to baseline ventricular pressures for comparative purposes in the setting of acute mitral regurgitation. Bold denotes *P*-value <0.05.

bpm: beats per minute; PVAN: posterior ventricular anchoring neochordal.
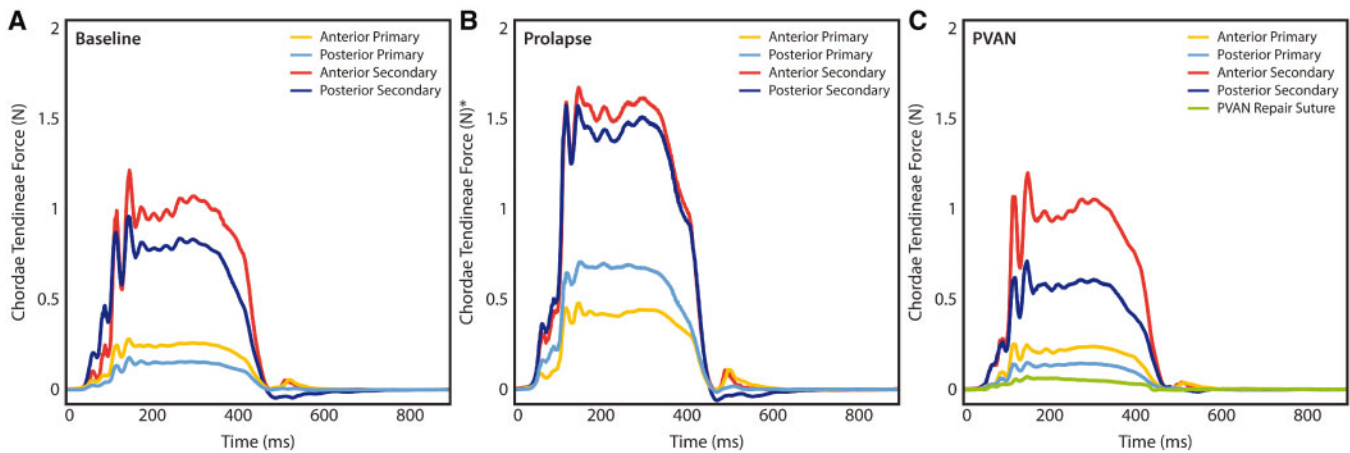
Figure 5: Composite force tracings for each group of chordae tendineae at baseline (**A**), after prolapse was induced (**B**) and following PVAN repair (**C**). PVAN repair resulted in normalization of forces to baseline levels for anterior primary, posterior primary, anterior secondary and posterior secondary chordae tendineae. The force tracing for the PVAN repair suture is also shown in (**C**), which experienced extremely low peak forces. *Prolapse tracings were normalized to baseline ventricular pressures for comparative purposes in the setting of acute mitral regurgitation. PVAN: posterior ventricular anchoring neochordal.
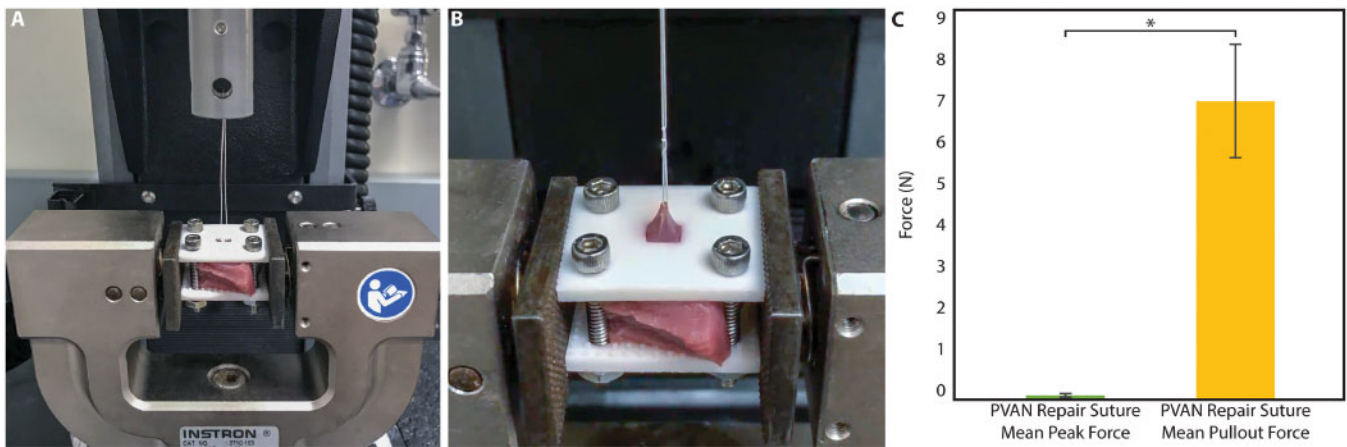
Figure 6: (**A** and **B**) Experimental set-up using uniaxial tensile testing machine to measure forces required to pull the repair suture from the posterior left ventricular myocardium. A 3D-printed clamp held the ventricular myocardial samples (*n* = 5) in place during experiments. (**C**) Results show that the average force required to pull the repair suture out of the posterior left ventricle is over 90 times higher than the average peak force experienced by the repair suture during normal physiological conditions (0.08 ± 0.04 N vs 6.90 ± 1.34 N, *P* < 0.001). PVAN: posterior ventricular anchoring neochordal.

anterior primary (0.23 ± 0.08 vs 0.37 ± 0.23 N, *P* = 0.046), posterior primary (0.14 ± 0.06 vs 0.62 ± 0.37 N, *P* = 0.001), anterior secondary (0.93 ± 0.38 vs 1.48 ± 0.52 N, *P* < 0.001) and posterior secondary (0.76 ± 0.28 vs 1.42 ± 0.69 N, *P* = 0.005). Following PVAN repair, forces returned to baseline levels in all conditions. Forces on the PVAN repair suture itself were minimal with mean peak forces of 0.08 ± 0.04 N, which is significantly less than even forces experienced by primary chordae in healthy valves (0.19 ± 0.08 N, *P* = 0.002). The force required to pull the PVAN repair suture free from the posterior ventricular tissue was significantly higher at 6.9 ± 1.3 N (*P* < 0.001, Fig. 6).

DISCUSSION

The PVAN repair is an effective technique for correcting MR secondary to posterior leaflet prolapse and requiring only a single suture makes the technique especially attractive for minimally invasive approaches. By positioning the imbricated and structurally optimized leaflet posteriorly, the PVAN repair suture effectively prevents SAM and maintains ideal leaflet height for maximal coaptation. In addition to restoring haemodynamic parameters, the PVAN repair normalizes chordae forces to baseline levels; whether this translates to enhanced durability of this technique over others is unknown. Unlike traditional neochord repairs anchored in the fibrous head of a papillary muscle, the PVAN suture is anchored in the posterior ventricular myocardium. A theoretical concern of PVAN repair is the strength of the ventricular anchor given that the repair relies on this suture. While the imbrication of excess leaflet tissue structurally optimizes the leaflet for coaptation to prevent leaflet prolapse, we hypothesized that the PVAN repair suture itself does not play a significant structural role in the repair, and like native primary chordae, serves to position the leaflet for ideal coaptation, after which point systolic forces are distributed throughout the mitral apparatus [12, 23, 24]. The results of our
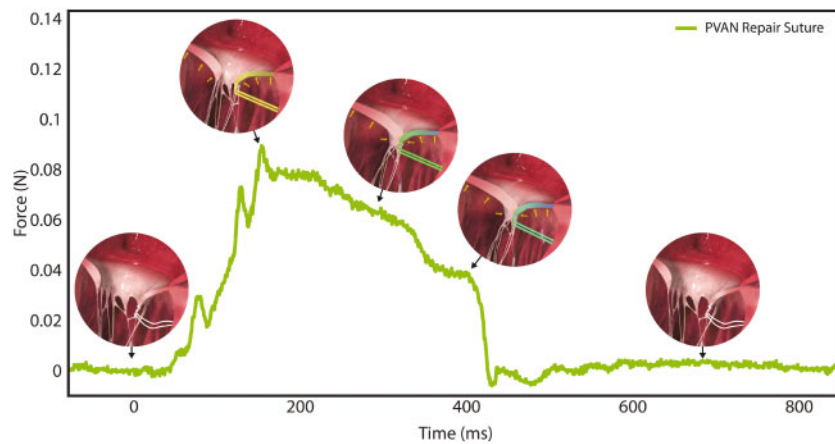
Figure 7: Close-up composite force tracing of the PVAN repair suture (note *y*-axis scale) overlaid with hypothesized renderings of PVAN repair suture forces. As predicted, forces during diastole are zero, peak in early-systole as the posterior leaflet is positioned for coaptation, after which point the forces are redistributed throughout the mitral valve apparatus and away from the PVAN suture, with marked reductions in PVAN repair suture forces throughout systole, until they fall to zero at the start of diastole. PVAN: posterior ventricular anchoring neochordal.

study support this hypothesis, with forces being nearly zero in diastole, peaking in early systole as the leaflet is positioned for coaptation, and then decreasing for the remainder of systole as forces are distributed throughout the valve apparatus (Fig. 7). We found that the force on the PVAN suture is extremely small, even compared to forces experienced by primary chordae of healthy valves, and the force required to tear the PVAN suture free from the posterior LV wall with resultant repair failure is over 90 times higher than the mean peak force on the repair suture. Although tissues experiencing cyclic stresses below their yield strength may still accumulate damage, the large discrepancy in suture force compared to pull-out force suggests that the strength of the posterior ventricular anchoring tissue and the forces exerted on the repair suture should not limit durability of this repair [25].

Other benefits of the PVAN technique include it being non-resectional; if during the operation the repair is felt to be inadequate, the repair suture can be modified, repositioned, or removed without damaging the leaflet. Resection, on the contrary, is irreversible and a suboptimal repair can result in unintended valve replacement [26]. Unlike traditional papillary muscle-based neochord repairs where precise suture length is required to prevent excessive leaflet tissue from causing SAM, the PVAN technique results in a posteriorly positioned leaflet, substantially reducing the risk of SAM [27]. No significant difference in effective orifice area when comparing baseline values to those following PVAN repair, though EOA did appear to trend downwards slightly, though not into ranges concerning for iatrogenic mitral stenosis as demonstrated by extremely low transmitral gradients in either group. Furthermore, we did not identify any significant differences in any other haemodynamic parameter when comparing the baseline and PVAN groups, which suggests that the magnitude of this downwards trend in EOA is unlikely to be large enough to have clinical significance. Lastly, the addition of an annuloplasty ring would also likely reduce EOA for any repair, regardless of surgical technique used. Future studies investigating the influence of annuloplasty ring on the PVAN repair, among many others, are currently underway.

Limitations

As an *ex vivo* investigation, our study does have some limitations in perfectly recreating the complex interactions between the annulus and ventricular components of the mitral valve apparatus, though our system does allow for native annular motion. The valves used in this study were also normal, healthy valves and P2 prolapse was induced by cutting chordae as opposed to natural pathological processes resulting in chordal rupture typical in degenerative valve disease. Nonetheless, this is an accepted model of MR commonly used experimentally [28, 29]. Future *in vivo* investigations currently underway will address some of these limitations. Lastly, we used porcine and not human valves. However, porcine and human mitral valves are remarkably similar, with the anterior leaflet attaching to approximately one-third of the annulus with a fibrous aortomitral curtain, the posterior leaflet attaching to the posterior two-thirds of the annulus, and the papillary muscles having comparable locations [30]. Chordae number and histological composition are also similar between these species [31]. As such, porcine mitral valves are realistic surrogates for human mitral valves in experiments not feasible in humans. While measuring forces on individual human valves *in vivo* is not currently possible, further validation using clinical outcomes data is indicated and currently underway.

CONCLUSION

This exploratory *ex vivo* study helps to provide biomechanical validation of the PVAN repair technique. In addition to restoring haemodynamic variables to baseline levels, PVAN repair results in normalization of chordae forces to baseline levels. By positioning the leaflet posteriorly, this technique is also extremely effective in preventing SAM. The theoretical concern regarding the strength of the repair suture and anchoring tissue in this technique should not be a limiting factor, as the forces experienced by the repair suture are extremely small relative to the maximum forces that can be supported by the posterior ventricular myocardium. Overall, the PVAN repair is an

effective, non-resectional, single-suture mitral valve repair technique that lends itself well to a minimally invasive approach and is biomechanically sound.

Funding

Conflict of interest: none declared.

Author contributions

Michael J. Paulsen: Conceptualization; Data curation; Formal analysis; Funding acquisition; Investigation; Methodology; Project administration; Resources; Software; Supervision; Validation; Visualization; Writing – original draft; Writing – review & editing. **Annabel M. Imbrie-Moore:** Conceptualization; Data curation; Formal analysis; Funding acquisition; Investigation; Methodology; Project administration; Resources; Software; Supervision; Validation; Visualization; Writing – original draft; Writing – review & editing. **Hanjay Wang:** Conceptualization; Funding acquisition; Investigation; Methodology; Writing – original draft; Writing – review & editing. **Jung Hwa Bae:** Conceptualization; Data curation; Investigation; Methodology; Resources; Software; Validation; Visualization; Writing – original draft; Writing – review & editing. **Camille E. Hironaka:** Data curation; Formal analysis; Investigation; Validation; Visualization; Writing – review & editing. **Justin M. Farry:** Data curation; Formal analysis; Investigation; Methodology; Software; Writing – review & editing. **Haley J. Lucian:** Data curation; Formal analysis; Investigation; Methodology; Software; Writing – review & editing. **Akshara D. Thakore:** Data curation; Formal analysis; Investigation; Methodology; Software; Writing – review & editing. **John W. MacArthur:** Conceptualization; Formal analysis; Methodology; Supervision; Writing – review & editing. **Mark R. Cutkosky:** Conceptualization; Data curation; Formal analysis; Investigation; Methodology; Project administration; Resources; Software; Supervision; Validation; Visualization; Writing – review & editing. **Y. Joseph Woo:** Conceptualization; Data curation; Formal analysis; Funding acquisition; Investigation; Methodology; Project administration; Resources; Software; Supervision; Validation; Visualization; Writing – original draft; Writing – review & editing.

REFERENCES

[1] Castillo JG, Anyanwu AC, Fuster V, Adams DH. A near 100% repair rate for mitral valve prolapse is achievable in a reference center: implications for future guidelines. J Thorac Cardiovasc Surg 2012;144:308–12.

[2] Goldstone AB, Cohen JE, Howard JL, Edwards BB, Acker AL, Hiesinger W *et al.* A "repair-all" strategy for degenerative mitral valve disease safely minimizes unnecessary replacement. Ann Thorac Surg 2015;99:1983–90; discussion 1990.

[3] Rosengart TK, Feldman T, Borger MA, Vassiliades TA, Gillinov AM, Hoercher KJ *et al.* Percutaneous and minimally invasive valve procedures: a scientific statement from the American Heart Association Council on Cardiovascular Surgery and Anesthesia, Council on Clinical Cardiology, Functional Genomics and Translational Biology Interdisciplinary Working Group, and Quality of Care and Outcomes Research Interdisciplinary Working Group. Circulation 2008;117: 1750–67.

[4] Davila JC, Glover RP, Trout RG, Mansure FS, Wood NE, Janton OH *et al.* Circumferential suture of the mitral ring; a method for the surgical correction of mitral insufficiency. J Thorac Surg 1955;30:531–60; discussion 560.

[5] Lillehei CW, Gott VL, Dewall RA, Varco RL. Surgical correction of pure mitral insufficiency by annuloplasty under direct vision. J Lancet 1957; 77:446–9.

[6] Hansen L, Winkel S, Kuhr J, Bader R, Bleese N, Riess F-C. Factors influencing survival and postoperative quality of life after mitral valve reconstruction. Eur J Cardiothorac Surg 2010;37:635–44.

[7] Mcgoon DC. Repair of mitral insufficiency due to ruptured chordae tendineae. J Thorac Cardiovasc Surg 1960.

[8] Carpentier A, Relland J, Deloche A, Fabiani J-N, D'Allaines C, Blondeau P *et al.* Conservative management of the prolapsed mitral valve. Ann Thorac Surg 1978;26:294–302.

[9] Asai T, Kinoshita T, Hosoba S, Takashima N, Kambara A, Suzuki T *et al.* Butterfly resection is safe and avoids systolic anterior motion in posterior leaflet prolapse repair. Ann Thorac Surg 2011;92:2097–102; discussion 2102.

[10] Brown ML, Abel MD, Click RL, Morford RG, Dearani JA, Sundt TM *et al.* Systolic anterior motion after mitral valve repair: is surgical intervention necessary? J Thorac Cardiovasc Surg 2007;133:136–43.

[11] Yoganathan AP, Lemmon JD, Kim YH, Levine RA, Vesier CC. A three-dimensional computational investigation of intraventricular fluid dynamics: examination into the initiation of systolic anterior motion of the mitral valve leaflets. J Biomech Eng 1995;117:94–102.

[12] Nazari S, Carli F, Salvi S, Banfi C, Aluffi A, Mourad Z *et al.* Patterns of systolic stress distribution on mitral valve anterior leaflet chordal apparatus. A structural mechanical theoretical analysis. J Cardiovasc Surg (Torino) 2000;41:193–202.

[13] Kuntze T, Borger MA, Falk V, Seeburger J, Girdauskas E, Doll N *et al.* Early and mid-term results of mitral valve repair using premeasured Gore-Tex loops ('loop technique'). Eur J Cardiothorac Surg 2008;33: 566–72.

[14] Neely RC, Borger MA. Myxomatous mitral valve repair: loop neochord technique. Oper Tech Thorac Cardiovasc Surg 2015;20:106–23.

[15] Woo YJ, MacArthur JW. Simplified nonresectional leaflet remodeling mitral valve repair for degenerative mitral regurgitation. J Thorac Cardiovasc Surg 2012;143:749–53.

[16] MacArthur JW, Cohen JE, Goldstone AB, Fairman AS, Edwards BB, Hornick MA *et al.* Nonresectional single-suture leaflet remodeling for degenerative mitral regurgitation facilitates minimally invasive mitral valve repair. Ann Thorac Surg 2013;96:1603–6.

[17] Shudo Y, Cohen JE, MacArthur JW, Goldstone AB, Hiraoka A, Howard J *et al.* Non-resectional leaflet remodeling mitral valve repair preserves leaflet mobility: a quantitative echocardiographic analysis of mitral valve configuration. Int J Cardiol 2015;186:16–18.

[18] Woo YJ, MacArthur JW. Posterior ventricular anchoring neochordal repair of degenerative mitral regurgitation efficiently remodels and repositions posterior leaflet prolapse. Eur J Cardiothorac Surg 2013;44:485–9; discussion 489.

[19] Paulsen MJ, Kasinpila P, Imbrie-Moore AM, Wang H, Hironaka CE, Koyano TK *et al.* Modeling conduit choice for valve-sparing aortic root replacement on biomechanics with a 3-dimensional-printed heart simulator. J Thorac Cardiovasc Surg 2018;158:392–403; discussions 404–7.

[20] Paulsen MJ, Bae JH, Imbrie-Moore AM, Wang H, Hironaka CE, Farry JM *et al.* Development and *ex vivo* validation of novel force-sensing neochordae for measuring chordae tendineae tension in the mitral valve apparatus using optical fibers with embedded Bragg gratings. J Biomech Eng 2019 (in press).

[21] Imbrie-Moore AM, Paulsen MJ, Thakore AD, Wang H, Hironaka CE, Lucian HJ *et al.* Ex vivo biomechanical study of apical versus papillary neochord anchoring for mitral regurgitation. Ann Thorac Surg 2019;108: 90–7; discussion 97–8.

[22] Rothman KJ. No adjustments are needed for multiple comparisons. Epidemiology 1990;1:43–6.

TRANSLATIONAL RESEARCH

[23] Lomholt M, Nielsen SL, Hansen SB, Andersen NT, Hasenkam JM. Differential tension between secondary and primary mitral chordae in an acute *in vivo* porcine model. J Heart Valve Dis 2002;11:337–45.

[24] Goetz WA, Lim H-S, Lansac E, Saber HA, Pekar F, Weber PA *et al.* Anterior mitral basal "stay" chords are essential for left ventricular geometry and function. J Heart Valve Dis 2005;14:195–202; discussion 202.

[25] Li W. Damage models for soft tissues: a survey. J Med Biol Eng 2016;36: 285–307.

[26] Lange R, Guenther T, Noebauer C, Kiefer B, Eichinger W, Voss B *et al.* Chordal replacement versus quadrangular resection for repair of isolated posterior mitral leaflet prolapse. Ann Thorac Surg 2010;89:1163–70; discussion 1170.

[27] Duebener LF, Wendler O, Nikoloudakis N, Georg T, Fries R, Schäfers HJ. Mitral-valve repair without annuloplasty rings: results after repair of anterior leaflet versus posterior-leaflet defects using polytetrafluoroethylene sutures for chordal replacement. Eur J Cardiothorac Surg 2000; 17:206–12.

[28] Leroux AA, Moonen ML, Pierard LA, Kolh P, Amory H. Animal models of mitral regurgitation induced by mitral valve chordae tendineae rupture. J Heart Valve Dis 2012;21:416–23.

[29] Li B, Cui Y, Zhang D, Luo X, Luo F, Li B *et al.* The characteristics of a porcine mitral regurgitation model. Exp Anim 2018;67:463–77.

[30] Crick SJ, Sheppard MN, Ho SY, Gebstein L, Anderson RH. Anatomy of the pig heart: comparisons with normal human cardiac structure. J Anatomy 1998;193(Pt 1):105–19.

[31] Millington-Sanders C, Meir A, Lawrence L, Stolinski C. Structure of chordae tendineae in the left ventricle of the human heart. J Anatomy 1998; 192: 573–81.